



University of Pennsylvania
ScholarlyCommons

Departmental Papers (CBE)

Department of Chemical & Biomolecular
Engineering

1-2006

Biphosphonate-Mediated Gene Vector Delivery from the Metal Surfaces of Stents

Ilia Fishbein

The Children's Hospital of Philadelphia

Ivan S. Alferiev

The Children's Hospital of Philadelphia

Origene Nyanguile

The Children's Hospital of Philadelphia

Richard Gaster


The Children's Hospital of Philadelphia

John M. Vohs

University of Pennsylvania, vohs@seas.upenn.edu

See next page for additional authors

Follow this and additional works at: http://repository.upenn.edu/cbe_papers

 Part of the [Biochemical and Biomolecular Engineering Commons](#), [Genetics and Genomics Commons](#), and the [Materials Science and Engineering Commons](#)

Recommended Citation

Fishbein, I., Alferiev, I. S., Nyanguile, O., Gaster, R., Vohs, J. M., Wong, G., Felderman, H., Chen, I., Choi, H., Wilensky, R. L., & Levy, R. J. (2006). Biphosphonate-Mediated Gene Vector Delivery from the Metal Surfaces of Stents. *PNAS (Proceedings of the National Academy of Sciences)*, 103 (1), 159-164. <http://dx.doi.org/10.1073/pnas.0502945102>

This paper is posted at ScholarlyCommons. http://repository.upenn.edu/cbe_papers/174

For more information, please contact repository@pobox.upenn.edu.

Biphosphonate-Mediated Gene Vector Delivery from the Metal Surfaces of Stents

Abstract

The clinical use of metallic expandable intravascular stents has resulted in improved therapeutic outcomes for coronary artery disease. However, arterial reobstruction after stenting, in-stent restenosis, remains an important problem. Gene therapy to treat in-stent restenosis by using gene vector delivery from the metallic stent surfaces has never been demonstrated. The present studies investigated the hypothesis that metal-biphosphonate binding can enable site-specific gene vector delivery from metal surfaces. Polyallylamine biphosphonate (PAA-BP) was synthesized by using Michael addition methodology. Exposure to aqueous solutions of PAA-BP resulted in the formation of a monomolecular biphosphonate layer on metal alloy surfaces (steel, nitinol, and cobalt-chromium), as demonstrated by x-ray photoelectron spectroscopy. Surface-bound PAA-BP enabled adenoviral (Ad) tethering due to covalent thiol-binding of either anti-Ad antibody or a recombinant Ad-receptor protein, D1. In arterial smooth muscle cell cultures, alloy samples configured with surface-tethered Ad were demonstrated to achieve site-specific transduction with a reporter gene, (GFP). Rat carotid stent angioplasties using metal stents exposed to aqueous PAA-BP and derivatized with anti-knob antibody or D1 resulted in extensive localized Ad-GFP expression in the arterial wall. In a separate study with a model therapeutic vector, Ad-inducible nitric oxide synthase (iNOS) attached to the biphosphonate-treated metal stent surface via D1, significant inhibition of restenosis was demonstrated (neointimal/media ration 1.68 ± 0.27 and 3.4 ± 0.35 ; Ad-iNOS vs. control, $P < 0.01$). It is concluded that effective gene vector delivery from metallic stent surfaces can be achieved using this approach.

Keywords

gene therapy, local delivery, restenosis

Disciplines

Biochemical and Biomolecular Engineering | Chemical Engineering | Engineering | Genetics and Genomics | Materials Science and Engineering

Author(s)

Ilia Fishbein, Ivan S. Alferiev, Origene Nyanguile, Richard Gaster, John M. Vohs, Gordon Sek-Yin Wong, Howard Felderman, I-Wei Chen, Hoon Choi, Robert L. Wilensky, and Robert J. Levy

Bisphosphonate-mediated gene vector delivery from the metal surfaces of stents

Ilia Fishbein*, Ivan S. Alferiev*, Origene Nyanguile*, Richard Gaster*, John M. Vohs[†], Gordon S. Wong[†], Howard Felderman*, I-Wei Chen[‡], Hoon Choi[‡], Robert L. Wilensky[§], and Robert J. Levy*[¶]

*Division of Cardiology, The Children's Hospital of Philadelphia, Departments of [†]Chemical and Biomolecular Engineering and [‡]Material Science and Engineering, and [§]The Cardiovascular Division, Hospital of the University of Pennsylvania, University of Pennsylvania, Philadelphia, PA 19104

Edited by Robert Langer, Massachusetts Institute of Technology, Cambridge, MA, and approved November 14, 2005 (received for review April 11, 2005)

The clinical use of metallic expandable intravascular stents has resulted in improved therapeutic outcomes for coronary artery disease. However, arterial reobstruction after stenting, in-stent restenosis, remains an important problem. Gene therapy to treat in-stent restenosis by using gene vector delivery from the metallic stent surfaces has never been demonstrated. The present studies investigated the hypothesis that metal-bisphosphonate binding can enable site-specific gene vector delivery from metal surfaces. Polyallylamine bisphosphonate (PAA-BP) was synthesized by using Michael addition methodology. Exposure to aqueous solutions of PAA-BP resulted in the formation of a monomolecular bisphosphonate layer on metal alloy surfaces (steel, nitinol, and cobalt-chromium), as demonstrated by x-ray photoelectron spectroscopy. Surface-bound PAA-BP enabled adenoviral (Ad) tethering due to covalent thiol-binding of either anti-Ad antibody or a recombinant Ad-receptor protein, D1. In arterial smooth muscle cell cultures, alloy samples configured with surface-tethered Ad were demonstrated to achieve site-specific transduction with a reporter gene, (GFP). Rat carotid stent angioplasties using metal stents exposed to aqueous PAA-BP and derivatized with anti-knob antibody or D1 resulted in extensive localized Ad-GFP expression in the arterial wall. In a separate study with a model therapeutic vector, Ad-inducible nitric oxide synthase (iNOS) attached to the bisphosphonate-treated metal stent surface via D1, significant inhibition of restenosis was demonstrated (neointimal/media ratio 1.68 ± 0.27 and 3.4 ± 0.35 ; Ad-iNOS vs. control, $P < 0.01$). It is concluded that effective gene vector delivery from metallic stent surfaces can be achieved by using this approach.

gene therapy | local delivery | restenosis

The use of balloon expandable metallic stents has resulted in improved therapeutic outcomes for coronary artery disease (1). However, stent angioplasty is complicated in many patients by reobstruction due to the formation of a neointima in the stented arterial segment, a disease process known as in-stent restenosis (2). The mechanisms responsible for in-stent restenosis involve proliferation and migration of medial smooth muscle cells (SMCs) and an associated increase in extracellular matrix components (2). The use of polymer-coated drug-eluting stents has markedly decreased the incidence of in-stent restenosis observed with unmodified metal stents (3). However, both experimental (4) and clinical (5) studies indicate a number of concerns about this approach, because polymer coatings on stents cause a more pronounced inflammatory response than metal surfaces (6), thus delaying rather than preventing restenosis (7, 8).

Polymer-coated gene-delivery stents have been demonstrated in animal studies to be effective for both reporter (9–13) and therapeutic (14, 15) vector delivery. Nevertheless, their use is problematic because of harmful properties of the polymer coatings (6, 7). Therefore, the present experiments investigated gene delivery directly from metal surfaces without the use of a polymer coating. Bisphosphonates are known to demonstrate high-affinity binding to both mineral and metallic surfaces through phosphonate-metal

coordination (16). It was therefore hypothesized that a metallic surface could be modified through an aminobisphosphonate exposure, thereby attaching to the metallic surface a derivatizable polybisphosphonate molecule that could, in turn, be covalently conjugated with vector-binding agents; this modification could, hypothetically, enable local gene delivery from metal surfaces exposed to the aqueous bisphosphonate. The present studies report (i) the synthesis of a unique water-soluble bisphosphonate, polyallylamine bisphosphonate (PAA-BP); (ii) binding interactions of aqueous PAA-BP with metal surfaces, thereby enabling the retention of a PAA-BP molecular monolayer that permits the attachment (via vector-binding molecules) and site-specific delivery of adenoviral vectors to cells in culture; and (iii) the efficacy of this approach using a replication-defective adenovirus (Ad) expressing inducible nitric oxide synthase (iNOS) as a model therapeutic gene for inhibiting in-stent restenosis in experimental animals.

Methods

Materials. Replication-defective type 5 (E1,E3-deleted) adenoviral vectors were obtained from the Gene Vector Core Facility of the University of Pennsylvania (Ad-GFP) and from the Gene Therapy Core Facility of the University of Iowa (Iowa City, IA) (Ad-iNOS). In both constructs, transgenes were under the control of the human cytomegalovirus promoter. Stainless steel (316L) foils and meshes were obtained from Goodfellow (Berwyn, PA) and Electron Microscopy Sciences (Hatfield, PA), respectively. Nitinol samples, cobalt-chromium alloy coupons, and 8-mm cobalt-chromium stents (SVS) were obtained under a material-transfer agreement from Cordis (Warren, NJ). The anti-knob antibody (IgG) used was a gift from Selective Genetics (San Diego).

Polymer Synthesis. For the synthesis of PAA-BP, two PAA (PAA) HCl salts, 15 kDa and 70 kDa, were obtained from Sigma-Aldrich; PAA relative molecular masses (mass average) were determined with size-exclusion chromatography by the manufacturer (Sigma-Aldrich). Vinylidene bisphosphonic acid tetrasodium salt was obtained from Rhodia, (Oldbury, U.K.). PAA base (from either PAA-HCl, 15 kDa, or PAA-HCl, 70 kDa, 23.6 mmol of NH_2 in both) and vinylidene-bisphosphonic acid (20 mmol) were combined in water, concentrated to a syrup (7.63 g), and heated at 100–110°C for 5 h. The reaction product was dissolved in water containing an excess of triethylamine, and pure solid PAA-BP was precipitated with an excess of HCl. Purified PAA-BP in the free-acid form was subjected to elemental analysis by using both combustion method-

Conflict of interest statement: No conflicts declared.

This paper was submitted directly (Track II) to the PNAS office.

Freely available online through the PNAS open access option.

Abbreviations: Ad, adenovirus; i-NOS, inducible isoform of nitric oxide synthase; PAA, polyallylamine; PAA-BP, PAA bisphosphonate; SMC, smooth muscle cell; SPDP, *N*-succinimidyl 3-(2-pyridyldithio) propionate; XPS, x-ray photoelectron spectroscopy.

[¶]To whom correspondence should be addressed at: The Children's Hospital of Philadelphia, Abramson Research Center, Suite 702, 3615 Civic Center Boulevard, Philadelphia, PA 19104-4318. E-mail: levyr@email.chop.edu.

© 2005 by The National Academy of Sciences of the USA

ology and proton-induced x-ray emission (Elemental Analysis, Lexington, KY) to determine composition and ^{31}P NMR to document purity.

Ad Immobilization and Release. For Ad binding, an anti-knob mouse monoclonal (IgG) antibody (2 mg/ml) was reduced with 2-mercaptoethylamine (10 mg/ml) at 37°C for 30 min and purified by gel filtration. The human recombinant D1 domain of the Coxsackie-Ad-receptor protein (CAR) was also used as a binding agent and was prepared as described in ref. 17, followed by the conjugation of eluted D1 thioester with cysteine (20 mg/ml).

Metallic surfaces were exposed to 3% aqueous PAA-BP, pH, 5.5, at 60°C for 4 h, exhaustively washed, and reacted with *N*-succinimidyl 3-(2-pyridylthio) propionate (SPDP, 20 mg/ml) for 1 h at 20°C. The higher molecular mass PAA-BP (using 70-kDa PAA) showed 20% lower metal-binding efficacy than did the lower molecular mass PAA-BP (using 15-kDa PAA) and thus was not further investigated. PAA-BP-treated SPDP-modified metallic samples were then reacted with reduced antibody or thiolated D1 for 12 h at 20°C under an argon atmosphere. Ad immobilization was attained by 3-hour incubations of antibody- or D1-derivatized metallic specimens in suspensions of 5×10^{10} Ad-GFP particles per ml in 5% BSA/PBS. Selected samples of Ad-GFP were rendered fluorescent by using a Cy3 modification as described in ref. 18 before immobilization. The amount of immobilized Ad was determined, by using a depletion assay, as the difference between the Cy3 fluorescent signal (540/580 nm) elicited from nondepleted and metal-sample-depleted virus suspensions.

To compare relative rates of Ad dissociation from the antibody- and D1-modified surfaces, meshes ($n = 4$ per group) configured with Cy3-labeled Ad linked via either antibody or D1 tethers were individually exposed to 350 μl of PBS. The incubation was carried out under shaking at 4°C for 1 week, with a daily change of buffer. Immediately after virus acquisition and at the end of the experiment, fluorescence micrographs of the meshes were taken under standardized settings of the camera. The digital images were analyzed by using mean luminescence intensity of Adobe PHOTOSHOP-generated histograms for the quantification of surface-attached Ad.

Surface Analyses. The x-ray photoelectron spectroscopy (XPS) spectra were collected at room temperature by using an Al K_{α} x-ray source (Vacuum Generators, Hastings, U.K.) and a hemispherical electron energy analyzer (Leybold, Hanau, Germany). Surface profiles were visualized by using a Dimension 3100 atomic-force microscope (Digital Instruments, Santa Barbara, CA). Imaging was performed in the intermittent noncontact (tapping) mode, by using oscillating linear Si tips with a resonance frequency range of 300–350 Hz. Each data scan was collected over a 25 μm^2 area at a scanning frequency of 0.50 Hz. Viral surface density, determined by counting five fields (1 μm^2), was expressed as mean \pm SE.

Cell-Culture Experiments. Rat aortic SMCs (A10 cells; American Type Culture Collection) were cultured to 90% confluence, as published in ref. 9. Equal amounts of free and either antibody-, or D1-conjugated mesh-immobilized Ad-GFP were added into wells of 24-well plates. The GFP expression was assessed after 48 h by fluorescence microscopy or by fluorimetry (485–535 nm) of cell lysates. All cell culture experiments were carried out in triplicate.

Rat Carotid Stent Angioplasty Study. Carotid stent angioplasties were carried out by using 8-mm stents (Cordis), as above, in male Sprague–Dawley rats (500–550 g, Taconic Farms) assigned to five experimental groups: (i) Metal stents not treated with PAA-BP (three rats) were compared with PAA-BP treated (but without Ad) stents (three rats) in 7-day studies comparing the inflammatory response in arterial wall between the two groups. (ii) A series (three rats) of 24-h explants examined the initial arterial-wall distribution

of stent-delivered (anti-knob-antibody-tethered) Cy3-labeled Ad-GFP. (iii) In 7-day reporter studies to assess the extent of transgene expression, rats were subjected to stent angioplasty using control (unmodified) metal stents (three rats) and antibody- (three rats) or D1-tethered (three rats) Ad-GFP PAA-BP stents. The estimated adenoviral load on each stent ranged from 2.5×10^9 to 6.3×10^9 particles. (iv) Ad-iNOS delivered for 16 days from stents was examined in efficacy studies comparing PAA-BP-only modified controls ($n = 7$), or PAA-BP-modified D1/Ad-iNOS ($n = 5$) stents. (v) Ad-GFP biodistribution after stent delivery by using D1/Ad-GFP (7-day study, $n = 5$) was assessed by PCR (see protocol below).

Morphometrical Methods. GFP expression was assessed by fluorescence microscopy and immunohistochemistry (19) with a primary monoclonal mouse anti-GFP antibody (Roche). Photomicrographs of four representative sections of each artery were obtained at $\times 200$ magnification by using a Leica DC 500 microscope digital-image acquisition system. The images were processed in Adobe PHOTOSHOP to eliminate background and converted into binary (black and white) images by using the program IMAGE (Scion, Frederick, MD). The area of “black” pixels, representing diaminobenzidine staining of the GFP-positive material, was divided by the total analyzed area and normalized to a percentage scale. Differences in the inflammatory response between PAA-BP-treated and bare-metal stents were compared by using hematoxylin and eosin staining and anti-CD68 (Serotec, Oxford, U.K.) immunostaining (20).

For the Ad-iNOS study, stented arterial segments were plastic-embedded (Technovit 9100, Wehrheim, Germany), sectioned, and stained by the Verhoff–van Giesen method. The arterial micrographs were captured as digital images (see above) under $\times 50$ magnification, and the areas of lumen, neointima, and media were calculated by using Scion IMAGE-generated tracings (see above) of the respective anatomic arterial compartments.

Biodistribution of GFP Expression by PCR. Ad-GFP stented and contralateral arteries and the samples of lung, myocardium, spleen, liver, and kidney were harvested. Phenol-chloroform DNA extraction was performed, and PCR amplification was carried out over 35 cycles with a PTC-200 PCR engine (MJ Research, Watertown, MA) by using GFP-specific primers (upstream, 5'-GGC TGC TGC AAA ACA GAT AC-3'; downstream, 5'-CGG ATC CTC TAG AGT CGA C-3'). Amplified samples were analyzed with agarose-gel electrophoresis using appropriate standards and positive controls (Ad-GFP-transduced A10 cells) as described in ref. 9.

Statistical Methods. Data are expressed as mean \pm SE. The significance of differences between means of experimental groups was determined by using Student *t* tests.

Results

A water-soluble PAA-BP that can both interact with metal-oxide surfaces and provide reactive sites for chemical conjugation was synthesized by a direct Michael addition of PAA to the activated double bond of vinylidene-bisphosphonic acid (Fig. 1A). The molecular mass of each allylamine hydrochloride unit (93.56) was used to calculate the number of reactive units in the 15,000-Da PAA-HCl polymer used in these studies as 160.3 units per polymer macromolecule, which were thereby available for bisphosphonate derivatization. In the initial formulation studied, the extent of modification with the bisphosphonate groups was calculated based on elemental analysis of precipitated pure PAA-BP in the free-acid form, which contained P, 17.7%, H, 6.45%, C, 29.9%, N, 6.18%, and O, 42.2%; thus, $\approx 65\%$ of PAA amine groups were calculated to be derivatized with bisphosphonate groups in this preparation. Furthermore, based on elemental analysis, the estimated molecular mass of PAA-BP is ≈ 30 kDa, as calculated by using the sums of the weights of modified (245.1 Da) and nonmodified (57.1 Da) allylamine residues. ^{31}P NMR of pure PAA-BP documented a single

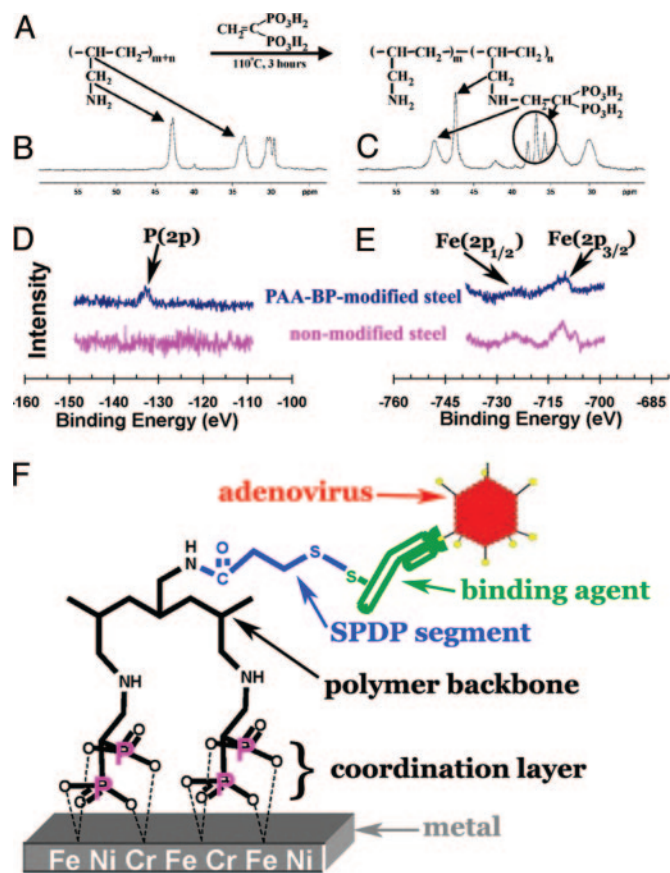


Fig. 1. The PAA-BP-synthesis reaction scheme (A) is shown with ^{13}C NMR spectra of PAA (B) and PAA-BP (C) demonstrating characteristic chemical shifts (43–50 ppm, *re. B* vs. C) with peak changes indicating bisphosphonate addition (C, *re. 47- and 50-ppm peaks*). XPS to detect phosphorus (D) and iron (E) on nonmodified and PAA-BP-modified steel surfaces demonstrates the appearance of P(2p) after PAA-BP treatment with persistent Fe(2p) signals. (F) A schematic representation is shown of the reversible Ad tethering to the PAA-BP-modified metal surface.

peak at δ 16 ppm. In the ^{13}C NMR spectrum of nonmodified PAA-HCl (Fig. 1B) three distinctive ^{13}C signals appear at $\delta \approx 30$ ppm (backbone CH_2), ≈ 34 ppm (backbone CH), and ≈ 43 ppm (pendant CH_2NH_2), whereas the ^{13}C NMR spectrum of PAA-BP (Fig. 1C) shows three new carbon moieties at ≈ 37 ppm (t, ≈ 112 Hz, CH of diphosphonoethyl groups), ≈ 47 ppm, and ≈ 50 ppm (pendant CH_2NH of modified links and CH_2 of diphosphonoethyl groups). Two additional formulations for vector-binding comparisons were synthesized by using the same PAA preparation described above but varying the amount of vinylidene-bisphosphonic acid to create a range of bisphosphonate modifications; elemental analyses demonstrated these two preparations to have 45% and 77% PAA amino groups modified.

Initial studies used stainless steel (316 L) coupons that were exposed to 3% aqueous PAA-BP (65% modified) and then rinsed exhaustively with water. XPS confirmed the presence of a PAA-BP molecular monolayer on the steel surface, demonstrating the emergence of a characteristic P(2p) signal (Fig. 1D) in the XPS of the treated sample, which persists after a 30-day incubation under simulated physiologic conditions (data not shown); a phosphorus signal is not present in the control 316 L steel (Fig. 1D). Furthermore, the characteristic Fe(2p) peaks of the steel substrate are still present in the XPS from the PAA-BP-modified sample (Fig. 1E), indicating that the thickness of the PAA-BP coordination layer is less than the effective XPS sampling depth (≈ 5 nm).

Table 1. PAA-BP-metal coordination bonding enables thiol-based covalent attachment of Ad-binding agents for tethering Ad: Ad-binding comparisons of various alloys and D1 vs. antibody (mean \pm SE)

Metal alloy	Anti-knob antibody-bound Ad ($\times 10^9$ particles per cm^2)	D1-bound Ad ($\times 10^9$ particles per cm^2)
316L steel	4.30 ± 0.34	$10.8 \pm 0.6^*$
Nitinol	5.27 ± 0.10	$11.6 \pm 0.4^*$
Co-Cr	3.52 ± 1.13	$15.1 \pm 1.37^*$

*Greater binding with D1, $P < 0.001$.

The primary amines of surface-bound PAA-BPs (45%, 65%, and 77% bisphosphonate-modified) were further reacted with a bifunctional (amino- and thiol-reactive) crosslinker, SPDP, to introduce thiol-reactive pyridyldithio groups to 316 L steel surfaces. To quantitate thiol-reactive functionalities, we reacted PAA-BP/SPDP-treated metal coupon samples with dansyl cysteine. Subsequent chemical reduction of the disulfide bond triggers dansyl release, which was used to quantitate fluorimetrically (355–535 nm) the thiol-reactive capacity of the surface-associated PAA-BP. All three candidate formulations were initially compared with 316 L steel binding studies using the dansyl cysteine assay. The results of these studies revealed the PAA-BP thiol-reactivity to be 54.5, 29.9, and 16.0 pmol/cm^2 for the 45%, 65%, and 77% BP modifications, respectively, corresponding to a minimal surface thiol-reactive density of 1 group per 10 nm^2 . Because the effective immobilization diameter of an Ig molecule exceeds 400 nm^2 (21), the theoretical achievable density of thiol-reactive groups is far beyond the minimal requirement for uniform protein surface modification, born out by the determination of Cy3-Ad attachment to differently treated steel foils by using PHOTOSHOP-generated histogram intensities of surface fluorescence (see *Methods*) as a relative index of immobilization density. These comparisons demonstrate virtually identical vector-binding levels for the various PAA-BP formulations (mean luminescence intensities 26.03 ± 5.93 , 26.52 ± 2.29 , and 25.19 ± 4.2 for 45%, 65%, and 77% BP modifications, respectively). Thus, the 65% modified PAA-BP was chosen as a lead formulation for subsequent *in vitro* and *in vivo* studies.

Exposure of either PAA-BP/anti-knob-antibody-conjugated or PAA-BP/D1-conjugated but not PAA-BP/SPDP-modified alloy samples to an adenoviral suspension resulted in affinity-mediated surface tethering of the Ads (Fig. 1F). The extent of Ad binding was quantitated by depletion assays (Table 1). These results revealed comparable levels of bound vector for the three alloy surfaces studied, with several-fold greater attachment for D1 (≈ 100 – 150 particles per μm^2 , Table 1) compared with the anti-knob antibody (≈ 35 – 50 particles per μm^2 , Table 1); no measurable vector was bound to either bare metal or PAA-BP-treated alloy samples without the use of either thiolated anti-knob antibody or D1. PAA-pretreated metallic samples subjected to the SPDP-D1 protocol described above demonstrated only trace levels of Cy3-vector binding (data not shown). The dissociation of Cy3-labeled Ad from the PAA-BP-binding-agents-primed meshes under sink conditions demonstrated a $37.4 \pm 2.5\%$ and $27.7 \pm 7.5\%$ decrease of surface-associated Ad for the antibody and D1 tethers, respectively ($P > 0.05$) after 1 week, indicating comparable rates of dissociation for D1 and antibody-mediated vector binding.

Atomic-force microscopy demonstrated multiple groupings of 100-nm-diameter units (Fig. 2A and B) that represent surface-bound Ads. This surface nanoparticulate pattern was not observed on steel samples exposed to only PAA-BP (Fig. 2C). Thus, affinity-mediated tethering of Ad allows for dense packing of the vector on a metal surface, estimated to be 19 ± 3 and 45 ± 2 viral particles per μm^2 (see Fig. 2A and B) for antibody- and D1-primed steel surfaces, respectively ($P < 0.001$, greater D1-mediated binding).

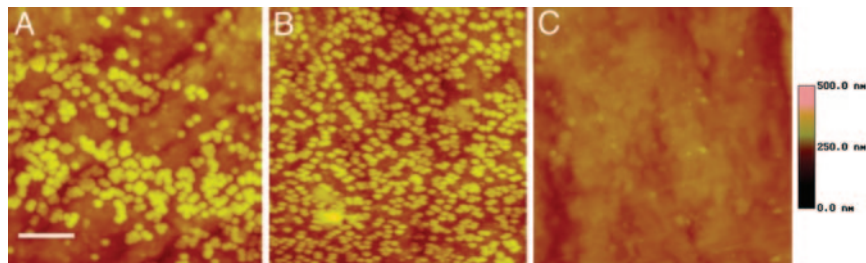


Fig. 2. Atomic-force microscopy of a PAA-BP/anti-knob antibody- (A) and D1- (B) derivatized stainless steel surface exposed to an Ad suspension (5×10^{10} particles per ml), demonstrating distribution of viral particles on the PAA-BP-activated surfaces. (C) For comparison, a control is shown consisting of a stainless steel surface exposed to only PAA-BP. (Scale bar, $1 \mu\text{m}$ and a depth scale of 500 nm is shown.)

These results are lower than the depletion assay data (Table 1), perhaps due to Ad loss during AFM-related procedures.

Stainless steel meshes configured with PAA-BP/antibody-immobilized GFP-encoding adenoviral vectors were placed in rat arterial SMC (A10 cells) cultures, resulting in intense highly localized transduction of $68.1 \pm 5.7\%$ of cells on the steel surface and within $50 \mu\text{m}$ of mesh borders (Fig. 3A). However, the same amount of free virus (2×10^8 particles) caused transduction of only $1.0 \pm 0.4\%$ cells throughout the cultures (Fig. 3B). The use of D1 for tethering resulted in 110-fold-higher levels of GFP expression after 48 h in A10 cell cultures than that achieved with anti-knob antibody (Fig. 3C).

Initial rat carotid stent angioplasty experiments compared a series of animals subjected to nonviral carotid stenting with ($n = 3$) and without ($n = 3$) stent pretreatment with aqueous PAA-BP. Hematoxylin and eosin staining demonstrated a mild inflammatory response due to stenting that did not differ between PAA-BP pretreatment and control bare-metal-stented arteries (results not shown). Because macrophages are the predominant cell type involved in the inflammatory process after stenting (22, 23), the sections were immunostained by using a rat macrophage-specific

anti-CD-68 antibody. Overall, the prevalence of CD-68-positive cells was higher for the arteries stented with bare metal stents ($45.02 \pm 16.83\%$; Fig. 4A) than PAA-BP-modified stents ($33.7 \pm 5.03\%$, Fig. 4B); however, this difference was not statistically significant ($P > 0.05$).

To examine the robustness of adenoviral attachment to the stent surface, Cy3-labeled Ad-GFP were immobilized on the PAA-BP pretreated, antibody-activated stents, and were shown to result in uniform vector association with stent struts (Fig. 4C). Twenty-four hours after stent deployment, Cy3-labeled Ads were observed at the stent/artery interface, as verified by *en face* fluorescence microscopy (Fig. 4D). The spatial pattern of the fluorescent signal noted in stented arterial segments *en face* corresponds to the shape of the stent struts (Fig. 4D), implying that the initial distribution of the virus in the vessel wall is governed by the physical imprint of the stent's wire surface. No fluorescent signal was elicited from the luminal surfaces of carotid arteries subjected to stent angioplasty with stents treated similarly but excluding the step of Cy3-labeled Ad exposure (Fig. 4E).

A series of rat carotid stent angioplasty studies with PAA-BP (\pm Ad-GFP) stents using either anti-knob antibody or D1 as vector-binding agents was carried out for 7 days. After quenching elastin autofluorescence with Evans blue, the GFP-positive cells were consistently demonstrated in the medial, neointimal, and adventitial layers of arteries treated with PAA-BP stents using either anti-knob antibody (Fig. 5A) or D1 (Fig. 5B) as binding agents for Ad-GFP attachment. The sections of arteries treated with control metal

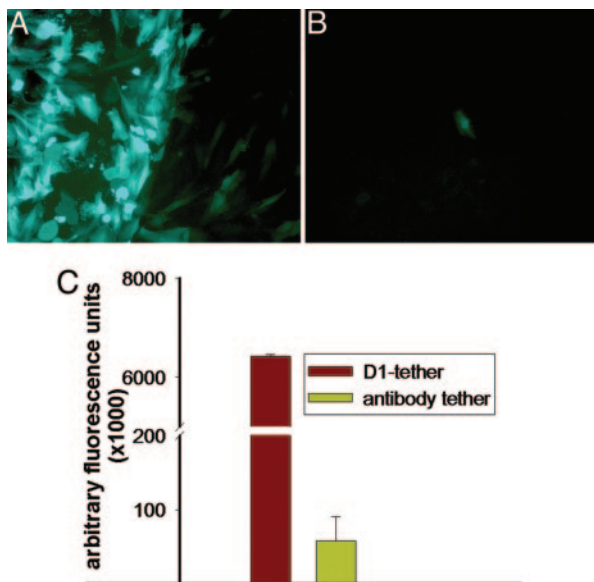


Fig. 3. GFP expression in cultured rat arterial SMCs (A10) transduced by the mesh-antibody-immobilized (A) or free (B) Ad-GFP (2×10^8 Ad particles) with prominent site-specific expression only with surface-immobilized vector (A). The multiplicity of infection was 1 for both cultures (magnification, $\times 100$, FITC filter set). (C) Fluorimetric assessment of GFP expression (485/510 nm) from A10 cell cultures transduced by Ad-GFP immobilized on the meshes by using anti-knob antibody vs. D1 with significantly greater GFP levels with D1 tethering ($P < 0.001$).

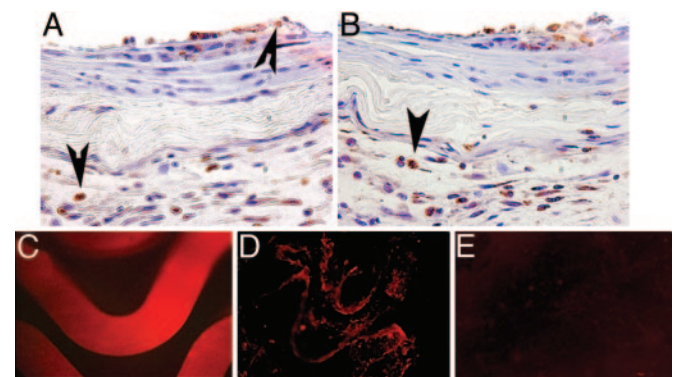


Fig. 4. PAA-BP-modified steel stents: Inflammatory response and tissue distribution of the vector *in vivo*. Representative DAB-immunohistochemistry photomicrographs, demonstrating prevalence of CD68-positive macrophages (indicated by the arrowheads) in arterial sections treated with bare metal (A) and PAA-BP-modified (B) stents (original magnification, $\times 200$). Fluorescent photomicrograph of a Cy3-Ad-modified stent surface (2.5×10^9 viral particles per stent) before deployment (C) and its imprint (*en face*) on the luminal surface of a rat carotid artery (D) 24 h after stenting. (E) Absence of autofluorescence in a rat carotid artery stented without tethered Ad. (C–E) Original magnification is $\times 200$, rhodamine filter set.

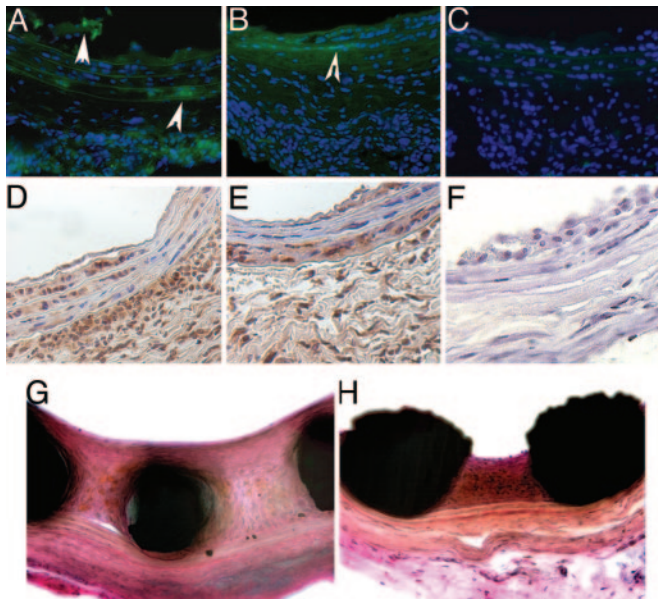


Fig. 5. PAA-BP-vector binding agent mediated tethering of Ad to steel surfaces *in vivo*: reporter (GFP) and Ad-iNOS therapeutic results. Fluorescence micrographs of rat carotid arteries treated with PAA-BP/antibody/Ad-GFP stents (A), PAA-BP/D1/Ad-GFP stents (B), or control bare stainless steel stents that show only residual autofluorescence (C). (A–C, where * indicates lumen) Original magnification, $\times 200$, FITC filter set. Arrowheads point to the GFP-positive cells. Peroxidase-based (diaminobenzidine, brown color) immunohistochemical detection of GFP expression in the stented carotid arterial segments harvested 7 days after stenting by using either Ad-GFP stent with antibody (D) and D1 (E) tethering or a control bare stainless steel stent (F). (D–F) original magnification, $\times 200$. Verhoeff–van Giessen-stained representative stented arterial sections of control bare metal (G) and Ad-iNOS/D1-derivatized (H) cobalt–chromium stents, demonstrating iNOS-mediated inhibition of restenosis. (G and H), original magnification, $\times 200$.

stents (without bisphosphonate pretreatment) did not demonstrate fluorescent cells (Fig. 5C). Widespread arterial-wall transduction was confirmed by anti-GFP immunostaining for both Ad-GFP tethered by anti-knob antibody (Fig. 5D) and D1 (Fig. 5E). Morphometric evaluation of the representative sections revealed comparable extensive transduction with GFP-positive cells in the medial, neointimal, and adventitial compartments of arteries from both experimental groups (Table 2). GFP-positive immunostaining (re. false positive) was not observed in arteries treated with control nonmodified bare-metal stents (Fig. 5F) not exposed to Ads. GFP-PCR biodistribution studies demonstrated GFP DNA after 35 cycles of amplification only in the arterial samples underlying the stents but not in the contralateral carotid arteries, liver, spleen, myocardium, and lungs (data not shown).

Therapeutic efficacy was demonstrated with PAA-BP-mediated metal-surface vector binding comparing unmodified metal stents

Table 2. Arterial GFP expression after stent-based delivery of Ad-GFP: morphometric results (anti-knob antibody- vs. D1-tethering for rat carotid stent reporter studies, mean \pm SE)

Ad attachment strategy	Neointima	Media	Adventitia
PAA-BP/antibody/Ad-GFP stents	37.9 \pm 20.3	6.8 \pm 1.6	19.6 \pm 5.6
PAA-BP/D1/Ad-GFP stents	23.0 \pm 6.4	8.7 \pm 4.5	16.4 \pm 1.0

Data represent percentage of GFP-positive area relative to the total area of the respective compartment in microscopic sections.

Table 3. Inhibition of in-stent restenosis with stent-delivery of Ad-iNOS: morphometric results (Ad-iNOS-D1-tethered vs. bare metal stents) for rat carotid stent angioplasty studies (mean \pm SE)

Group	Neointima, mm ²	Neointima/media	Stenosis, %
iNOS	0.23 \pm 0.02	1.68 \pm 0.27	23.1 \pm 3.4
Control	0.40 \pm 0.04	3.34 \pm 0.35	40.7 \pm 4.2
Statistical power (t-test)	<i>P</i> = 0.011	<i>P</i> = 0.006	<i>P</i> = 0.013

with the same stents with aqueous PAA-BP/D1 exposure by using Ad-iNOS as a model therapeutic gene vector. The Ad-iNOS gene-delivery-stent arteries demonstrated a significant therapeutic effect with diminished in-stent restenosis compared with controls, as verified by morphometric results quantitating neointimal area, neointimal-to-medial-area ratios, and differences in the percent of luminal stenosis (see Table 3 and Fig. 5 G and H).

Discussion

These results demonstrate successful delivery of a gene vector from a metal surface treated with an aqueous bisphosphonate solution to enable tethering. The data also show that the aqueous polybisphosphonate–metal-binding interaction used to attach Ad vectors occurs with a variety of alloys and thereby enables comparable levels of covalent attachment of vector-binding agents for gene delivery. These studies have also shown that various vector-binding agents can be used for gene delivery, such as anti-Ad antibodies, or recombinant proteins, such as D1, a recombinant Ad-receptor fragment. Importantly, this gene-delivery strategy can be used efficaciously to treat in-stent restenosis, as demonstrated by the Ad-iNOS results (Table 3).

Catheter delivery of both viral (24) and nonviral (25) gene therapeutics has been previously investigated for the mitigation of in-stent restenosis. Adaptation of the stent itself as a platform for gene delivery has a number of important advantages. First, animal and clinical studies have consistently shown that mural thrombosis and arterial SMC proliferation occur predominantly near stent struts (26). Thus, a relatively small amount of stent-immobilized gene vectors strategically placed at the interface of tissue and implant might be sufficient to produce a clinically significant therapeutic transduction of regional cells. Second, stent-tethered vectors that are physically shielded from the shearing effect of blood flow can, hypothetically, persist in tissues. Indeed, our Cy3-labeled Ad studies (Fig. 4D) revealed the deposition of fluorescent-labeled virus beneath the struts 24 h after stenting, despite active blood flow. Thirdly, immobilization of Ad vectors on stents diminishes distal spread of the vectors to nontarget tissues, as our PCR data show.

The mechanisms of Ad delivery from metal surfaces in the present studies, both *in vitro* and *in vivo*, must involve dissociation of the vector from the PAA-BP–binding-agent complex before cell uptake. The cell culture studies demonstrate a site-specific localization of GFP expression to the region of the PAA-BP-treated metal mesh (Fig. 3A), whereas the *in vivo* results show GFP expression deep in the media and adventitia of the artery (Fig. 5). This difference is likely because of a number of factors, including Ad transduction of arterial SMCs in close proximity to the stent struts, followed by migration of these cells during the early formation of a neointima and the forceful compression of vector into the arterial wall, as shown in Fig. 4D. Intact arterial elastic laminae are considered to be virtually impenetrable for adenoviral particles (27). However, stenting causes multiple lacerations of the elastic laminae, thus facilitating egress of the vector into the adventitial compartment. The cellular types within the adventitia (mainly

fibroblasts and myofibroblasts) are known to be more susceptible to adenoviral transduction than medial SMC (28), perhaps explaining the high extent of transduction in the adventitia observed in our reporter studies (Table 2). Considering the active role the adventitia plays in the formation of neointimal lesions (29), the ability of the stent-delivery approach investigated herein to transduce cells in the adventitia might be therapeutically relevant. Importantly, the penetration of the vector into the adventitia did not result in the dissemination of the virus beyond the stented arterial segment, as verified by the GFP-PCR results.

In addition, the results of *in vitro* studies show a greater Ad-binding capacity of D1 vs. anti-knob antibody (Fig. 2 and Table 1) and a significantly higher level of gene expression in cell culture with D1-tethered Ad (Fig. 3). These differences may be due to both a higher Ad binding affinity of immobilized D1 vs. the antibody used and subsequent facilitated processing of the Ad-D1-receptor complex. The reported dissociation constant (K_d) (in solution) for the anti-knob antibody used in our study is 0.31 nM (17); however, this value might be lower for the immobilized, chemically reduced molecule (30). Our Ad-release studies, carried out in an acellular system, demonstrated a somewhat higher dissociation rate for virus tethered via anti-knob antibody vs. D1-tethered Ad, confirming tighter binding with the immobilized receptor protein. Furthermore, it has been shown that the initial binding event of Ad to immobilized dimeric D1 has a much lower affinity ($K_d = 20$ nM) than an observed secondary binding event ($K_d = 1$ nM), thus suggesting that conformational changes of covalently attached D1 could actually facilitate more rapid release of Ad than would be otherwise expected (31). Thus, higher Ad binding with D1 tethering and facilitated release/transduction in the presence of cells are not mutually exclusive.

iNOS was chosen as a model therapeutic gene for these studies because of its previous efficacious use in delivery-catheter gene-therapy studies with a pig coronary stent angioplasty model (24) and the fact that iNOS can inhibit SMC proliferation (32, 33) and migration (34), platelet activation (35), and extracellular-matrix production (32). Thus, the therapeutic potential of iNOS is far broader than any of the current pharmaceuticals used with drug-eluting stents. Other types of gene vectors could be attached through binding agents comparable with those used in the present studies for Ads. To this end, high-affinity receptors for adeno-associated viruses (36) and retroviruses (37) have been described and cloned and, thus, could hypothetically be used with PAA-BP as described herein.

It is concluded that pretreatment of metal alloy surfaces with an aqueous bisphosphonate solution, PAA-BP, enables vector binding to bare metal through the formation of a surface-oriented PAA-BP-metal-coordination complex. This metal-bisphosphonate-coordination complex has been demonstrated in the present studies to enable the covalent attachment of vector-binding agents for therapeutic gene delivery to the arterial wall. Because of the widespread use of metallic implants in medicine, these results have broad implications for a therapeutic approach involving implantable medical devices configured with gene-therapy constructs.

We thank Mrs. Jeanne Connolly for her assistance in preparing the figures for this article, Ms. Jennifer LeBold for manuscript preparation, and Cordis, Inc. (Warren, NJ) for donating stents through a material-transfer agreement. This work was supported, in part, by National Heart, Lung, and Blood Institute Grant HL 72108; a grant from the Nanotechnology Institute; and both the William J. Rashkind Endowment and Erin's Fund of The Children's Hospital of Philadelphia.

- Belli, G., Ellis, S. G. & Topol, E. J. (1997) *Progr. Cardiovasc. Dis.* **40**, 159–182.
- Lowe, H. C., Oesterle, S. N. & Khachigian, L. M. (2002) *J. Am. Coll. Cardiol.* **39**, 183–193.
- Fattori, R. & Piva, T. (2003) *Lancet* **361**, 247–249.
- Farb, A., Heller, P. F., Shroff, S., Cheng, L., Kolodgie, F. D., Carter, A. J., Scott, D. S., Froehlich, J. & Virmani, R. (2001) *Circulation* **104**, 473–479.
- Serruys, P. W., Degertekin, M., Tanabe, K., Abizaid, A., Sousa, J. E., Colombo, A., Guagliumi, G., Wijns, W., Lindeboom, W. K., Ligthart, J., et al. (2002) *Circulation* **106**, 798–803.
- van der Giessen, W. J., Lincoff, A. M., Schwartz, R. S., van Beusekom, H. M., Serruys, P. W., Holmes, D. R., Jr., Ellis, S. G. & Topol, E. J. (1996) *Circulation* **94**, 1690–1697.
- Carter, A. J., Aggarwal, M., Kopia, G. A., Tio, F., Tsao, P. S., Kolata, R., Yeung, A. C., Llanos, G., Dooley, J. & Falotico, R. (2004) *Cardiovasc. Res.* **63**, 617–624.
- Sousa, J. E., Costa, M. A., Farb, A., Abizaid, A., Sousa, A., Seixas, A. C., da Silva, L. M., Feres, F., Pinto, I., Mattos, L. A. & Virmani, R. (2004) *Circulation* **110**, e5–e6.
- Klugherz, B. D., Jones, P. L., Cui, X., Chen, W., Meneveau, N. F., DeFelice, S., Connolly, J., Wilensky, R. L. & Levy, R. J. (2000) *Nat. Biotechnol.* **18**, 1181–1184.
- Klugherz, B. D., Song, C., DeFelice, S., Cui, X., Lu, Z., Connolly, J., Hinson, J. T., Wilensky, R. L. & Levy, R. J. (2002) *Hum. Gene Ther.* **13**, 443–454.
- Nakayama, Y., Ji-Youn, K., Nishi, S., Ueno, H. & Matsuda, T. (2001) *J. Biomed. Mater. Res.* **57**, 559–566.
- Perlstein, I., Connolly, J. M., Cui, X., Song, C., Li, Q., Jones, P. L., Lu, Z., DeFelice, S., Klugherz, B., Wilensky, R., et al. (2003) *Gene Ther.* **10**, 1420–1428.
- Takahashi, A., Palmer-Opolski, M., Smith, R. C. & Walsh, K. (2003) *Gene Ther.* **10**, 1471–1478.
- Johnson, T. W., Wu, Y. X., Herdeg, C., Baumbach, A., Newby, A. C., Karsch, K. R., Oberhoff, M., Johnson, T. & Karsch, K. K. (2005) *Arterioscler. Thromb. Vasc. Biol.* **25**, 754–759.
- Walter, D. H., Cejna, M., Diaz-Sandoval, L., Willis, S., Kirkwood, L., Stratford, P. W., Tietz, A. B., Kirchmair, R., Silver, M., Curry, C., et al. (2004) *Circulation* **21**, 21.
- van Alsten, J. G. (1999) *Langmuir* **15**, 7605–7614.
- Nyanguile, O., Dancic, C., Blakemore, J., Mulgrew, K., Kaleko, M. & Stevenson, S. C. (2003) *Gene Ther.* **10**, 1362–1369.
- Leopold, P. L., Ferris, B., Grinberg, I., Worgall, S., Hackett, N. R. & Crystal, R. G. (1998) *Hum. Gene Ther.* **9**, 367–378.
- Du, X., Yang, Y., Le Visage, C., Chen, H. H., DeJong, R., Qiu, B., Wang, D., Leong, K. W., Hamper, U. M. & Yang, X. (2003) *Radiology* **228**, 555–559.
- Danenberg, H. D., Fishbein, I., Epstein, H., Waltenberger, J., Moerman, E., Monkkonen, J., Gao, J., Gathi, I., Reichl, R. & Golomb, G. (2003) *J. Cardiovasc. Pharmacol.* **42**, 671–679.
- Wang, Z. & Jin, G. (2003) *J. Biochem. Biophys. Methods* **57**, 203–211.
- Welt, F. G. & Rogers, C. (2002) *Arterioscler. Thromb. Vasc. Biol.* **22**, 1769–1776.
- Finn, A. V., Gold, H. K., Tang, A., Weber, D. K., Wight, T. N., Clermont, A., Virmani, R. & Kolodgie, F. D. (2002) *J. Vasc. Res.* **39**, 414–425.
- Wang, K., Kessler, P. D., Zhou, Z., Penn, M. S., Forudi, F., Zhou, X., Tarakji, K., Kibbe, M., Kovetski, I., Brough, D. E., et al. (2003) *Mol. Ther.* **7**, 597–603.
- Muhs, A., Heublein, B., Schletter, J., Herrmann, A., Rudiger, M., Sturm, M., Grust, A., Malm, J., Schrader, J. & Von Der Leyen, H. E. (2003) *Hum. Gene Ther.* **14**, 375–383.
- Yutani, C., Ishibashi-Ueda, H., Suzuki, T. & Kojima, A. (1999) *Cardiology* **92**, 171–177.
- Rome, J. J., Shayani, V., Flugelman, M. Y., Newman, K. D., Farb, A., Virmani, R. & Dichek, D. A. (1994) *Arterioscler. Thromb. Vasc. Biol.* **14**, 148–161.
- Rios, C. D., Ooboshi, H., Piegors, D., Davidson, B. L. & Heistad, D. D. (1995) *Arterioscler. Thromb. Vasc. Biol.* **15**, 2241–2245.
- Wilcox, J. N., Cipolla, G. D., Martin, F. H., Simonet, L., Dunn, B., Ross, C. E. & Scott, N. A. (1997) *Ann. N.Y. Acad. Sci.* **811**, 437–447.
- Hermanson, G. T. (1996) *Bioconjugate Techniques* (Academic, San Diego), pp. 456–493.
- Lortat-Jacob, H., Chouin, E., Cusack, S. & van Raaij, M. J. (2001) *J. Biol. Chem.* **276**, 9009–9015.
- Rizvi, M. A. & Myers, P. R. (1997) *J. Mol. Cell. Cardiol.* **29**, 1779–1789.
- Sarkar, R., Gordon, D., Stanley, J. C. & Webb, R. C. (1997) *Am. J. Physiol.* **272**, H1810–H1818.
- Sarkar, R., Meinberg, E. G., Stanley, J. C., Gordon, D. & Webb, R. C. (1996) *Circ. Res.* **78**, 225–230.
- Nong, Z., Hoylaerts, M., Van Pelt, N., Collen, D. & Janssens, S. (1997) *Circ. Res.* **81**, 865–869.
- Qing, K., Mah, C., Hansen, J., Zhou, S., Dwarki, V. & Srivastava, A. (1999) *Nat. Med.* **5**, 71–77.
- Kwong, P. D., Wyatt, R., Robinson, J., Sweet, R. W., Sodroski, J. & Hendrickson, W. A. (1998) *Nature* **393**, 648–659.